Acta Biomaterialia 142 (2022) 149–159

Contents lists available at ScienceDirect

Acta Biomaterialia

journal homepage: www.elsevier.com/locate/actbio

Full length article

Cell alignment modulated by surface nano-topography – Roles of cell-matrix and cell-cell interactions

Stephen Coyle[a], Bryant Doss[b], Yucheng Huo[b], Hemang Raj Singh[b], David Quinn[a,*], K. Jimmy Hsia[b,c,**], Philip R. LeDuc[a,d,e,f,g,*]

[a] Department of Mechanical Engineering, Carnegie Mellon University, Pittsburgh, PA 15213, United States
[b] School of Mechanical & Aerospace Engineering, Nanyang Technological University, Singapore
[c] School of Chemical & Biomedical Engineering, Nanyang Technological University, Singapore
[d] Department of Biomedical Engineering, Carnegie Mellon University, Pittsburgh, PA 15213, United States
[e] Department of Biological Sciences, Carnegie Mellon University, Pittsburgh, PA 15213, United States
[f] Department of Computational Biology, Carnegie Mellon University, Pittsburgh, PA 15213, United States
[g] Department of Electrical and Computer Engineering, Carnegie Mellon University, Pittsburgh, PA 15213, United States

ARTICLE INFO

Article history:
Received 4 June 2021
Revised 19 January 2022
Accepted 31 January 2022
Available online 4 February 2022

Keywords:
N-cadherin
Alignment
Topography
Mechanotransduction
Cell motility

ABSTRACT

The propensity of cells to align in particular directions is relevant to a number of areas, including tissue engineering and biohybrid robotics. Cell alignment is modulated through various extracellular conditions including surface topographies, mechanical cues from cell-matrix interactions, and cell-cell interactions. Understanding of these conditions provides guidance for desirable cellular structure constructions. In this study, we examine the roles of surface topographies and cell-cell interactions in inducing cell alignment. We employed wavy surface topographies at the nanometer scale as a model extracellular environment for cell culture. The results show that, within a certain range of wavelengths and amplitudes of the surface topographies, cell alignment is dependent on cell confluency. This dependence on both topology and confluency suggests interplay between cell-cell and cell-matrix interactions in inducing cell alignment. Images of sparsely distributed and confluent cells also demonstrated clear differences in the structures of their focal adhesion complexes. To understand this effect, we introduced anti-N-cadherin to cell culture to inhibit cell-cell interactions. The results show that, when anti-N-cadherin was applied, cells on wavy surfaces required greater confluency to achieve the same alignment compared to that in the absence of anti-N-cadherin. The understanding of the cell alignment mechanisms will be important in numerous potential applications such as scaffold design, tissue repair, and development of biohybrid robotic systems.

Statement of significance

Cell alignment plays a critical role in numerous biological functions. Advances in tissue engineering utilizes cell alignment to restore, maintain, or even replace different types of biological tissues. The clinical impact that tissue engineering has made is facilitated by advancements in the understanding of interactions between scaffolds, biological factors, and cells. This work further elucidates the role of cell-cell interactions in promoting the organization of biological tissues.

1. Introduction

Work in tissue engineering is frequently aimed at controlling the alignment of cells in 2D or 3D cultures in vitro to recapitulate microstructures of native tissues in vivo. Cell alignment plays a critical role in numerous biological functions from the formation of skeletal muscular tissue during embryonic development to maintaining vascular health as an adult. Therefore, effective methods to replicate biological functions in tissue engineering necessitates

* Corresponding authors: Department of Mechanical Engineering, Carnegie Mellon University, 5000 Forbes Ave, Pittsburgh, PA 15213, United States.
** Corresponding authors: School of Mechanical & Aerospace Engineering, Nanyang Technological University, 50 Nanyang Avenue, 639798, Singapore.
E-mail addresses: djquinn@andrew.cmu.edu (D. Quinn), kjhsia@ntu.edu.sg (K. Jimmy Hsia), prl@andrew.cmu.edu (P.R. LeDuc).

https://doi.org/10.1016/j.actbio.2022.01.057

cell alignment. The clinical impact of cell alignment in tissue engineering has been articulated in a diversity of physiological systems from skin to heart to bone tissue [1–3]. At the intersection of cell alignment in tissue engineering is cell-substrate interactions, cell-cell interactions, and biological factors which are critical considerations for the design of engineered biomaterials designed to interface and integrate with tissues For example, Sawa et al. has treated dilated cardiomyopathy in more than 40 patients by transplanting tissue engineered myoblast sheets [4]. In their study, interactions between cells and temperature-responsive substrates allowed for the controlled release and transplant of a monolayers of cells directly onto failed myocardium. Cell-cell junctions maintained the myoblast sheet integrity, and the biological factors between the transplanted myoblast sheets and cardiomyocytes facilitated fibrosis, angiogenesis, and local recruitment of stem cells. The transplanted engineered myoblast sheets improved cardiac function sufficiently to discontinue patient need of using left ventricular assist systems.

Cell-substrate interactions facilitate cell alignment through focal adhesion the binding processes between cell transmembrane molecules and the substrate. Cell adhesion can be enhanced by extracellular matrix (ECM) absorption on the substrate surface resulting in cell-matrix adhesions. In this study, we focus on cell-matrix adhesion on fibronectin. One technique that can be used to modulate cell alignment on substrates is the introduction of anisotropy. Anisotropy has been used in various ways to induce cell alignment such as in topographical arrangement of geometric patterns, in stiffness gradients on scaffolds, and in the alignment of ECM networks surrounding cells. These techniques can be utilized in fabricating scaffolds on which cells grow into morphologies more closely resembling conditions in vivo [5–15]. Our work is focused on anisotropic geometric patterns and its impact on cell responses. In particular, we investigate the effects of surface waviness on alignment of elongated cells.

The synthesis of tissues in these and related fields requires a fundamental understanding of the roles of ECM and mechanotransduction, which are essential in the formation and functionalities of engineered tissues. Such understanding requires comprehensive studies of how cells interact with ECM either as individual cells or collectively as cell constructs/micro-tissues [11].

The effects of anisotropic geometric patterns on cell-ECM surface interactions have been investigated by controlling the surfaces to which cells adhered. For example, mouse skeletal muscle cells (C2C12 cells), when seeded on sinusoidal surfaces with wavelengths ranging from sub-micrometer to micrometer scale, aligned along the direction of the wavy patterns [12,16]. In a previous study, Grigola et al. found that depending on the parameters of the sinusoidal wave (wavelength, amplitude, curvature, etc.), cells exhibited alignment either individually or after reaching a level of confluency [17]. The study found that both cell-ECM interaction and cell-cell interaction have a role in cell alignment in 2D culture in vitro [17]. Furthermore, an alignment sensitivity parameter was proposed to characterize sinusoidal wavy topographies that led to cell-matrix interactions [17].

Cell alignment to topographical surface features is facilitated by mechanotransduction. Mechanotransduction is the process by which mechanical stimuli activate biochemical reactions and cellular responses, leading to gene expression, protein synthesis, and phenotypic change [18]. Mechanosensors and signal transduction are integral mechanisms of mechanotransduction that influence cell morphology and are affected by cell-matrix interactions [19–22]. Mechanotransduction mechanisms for cell-matrix interactions and cell-cell interactions are similar but distinct [23]. The strengths of cell-matrix interaction and cell-cell interaction may be correlated, either positively or negatively. Following the work of Grigola et al. [17], the objective of the current study is to gain a more in-depth understanding of the roles of cell-matrix and cell-cell interactions when sensing the geometric patterns of ECM surfaces.

To examine cell alignment in response to surface topography and cell-cell interactions, we developed controlled surface topographies on biocompatible polydimethylsiloxane (PDMS). We cultured cells on these nano-topographies to understand the effects of topography on cell alignment. We also introduced polyclonal anti-N-cadherin to inhibit cell-cell interactions to understand the impact of cell-matrix interactions on cell alignment (Fig. 1). The effect of anti-N-cadherin was analyzed by comparing individual cell morphology and cell motility on patterned scaffolds with or without the anti-body. A sensitivity parameter was then implemented to understand the changes in cell response on controlled scaffolds. Furthermore, time lapse imaging allowed us to compare the impact of time and confluency during cell alignment.

2. Materials and methods

2.1. Sinusoidal topography substrates

A regular standing-sinusoidal wave pattern across the entire area for the cell culture was created (Fig. 2). While PDMS wrinkling and soft lithography can be used to fabricate sinusoidal wave patterns [24–26], in this work, surface topographies on PDMS (Sylgard 184, Dow Corning) were fabricated through casting using commercially available holographic diffraction gratings. Holographic diffraction gratings (Edmund Optics #43–775, #54–509, #40–267) were used as templates for molding PDMS. PDMS was mixed at a 10:1 ratio, degassed, then a small drop was sandwiched between an oxygen plasma cleaned glass coverslip and the template with a weight on top, degassed again, cured at 60° overnight for plastic templates or 37° overnight for glass templates, then the coverslip and template were gently separated leaving a thin PDMS layer on the coverslip; PDMS samples made from glass templates were further cured at 60° and flat PDMS samples were produced in a similar manner by using the reverse side of the plastic templates. Sinusoidal wavelengths and amplitudes were measured by atomic force microscopy to be: λ=2 μm with d∼170 nm, λ=1 μm with d∼130 nm, and λ=0.56 μm with d∼150 nm. Substrates were sterilized with 70% ethanol for 30 min, exposed to UV germicidal light for 1 hour in a biosafety cabinet, then incubated with 10 μg/ml fibronectin (Corning 356,008) in PBS for 1 hour at 37° Following this, the fibronectin solution was removed, and substrates were washed with PBS and complete growth media was added in preparation for cell seeding. The PDMS molding sometimes results in reduced amplitude of the grating due to the fragility of the grating. The change in amplitude, however, allows for the scaffolds with differing aspect ratios to be used with cell culture [16].

2.2. Time lapse imaging

C2C12 cells (American Type Culture Collection - ATCC) were seeded on the patterned side of the PDMS scaffolds at 10,000 cells/cm^2. Cells were cultured in Dulbecco's Modified Eagle Medium (DMEM, ThermoFisher 11,995,065) supplemented with 10% Fetal Bovine Serum (ATCC 30–2020) and 1% Penicillin (ATCC 30–2300). Cells in the presence of anti-N-cadherin (Thermofisher PA5–29,570) were cultured at a concentration of 5 μg/ml. After one hour, cells were treated either with or without the presence of anti-N-cadherin antibodies for 48 to 72 h while being cultured in the Zeiss Large Incubation Chamber XL-S1. Cell media was replaced every 24 h. Time lapse images were compared between cell cultures using images captured with a 10x objective on a Zeiss AxioObserver Z1 Phase Contrast Microscope. Time lapse intervals were every 15 min. Cell migration was tracked using the ImageJ plugin MTrackJ [27].

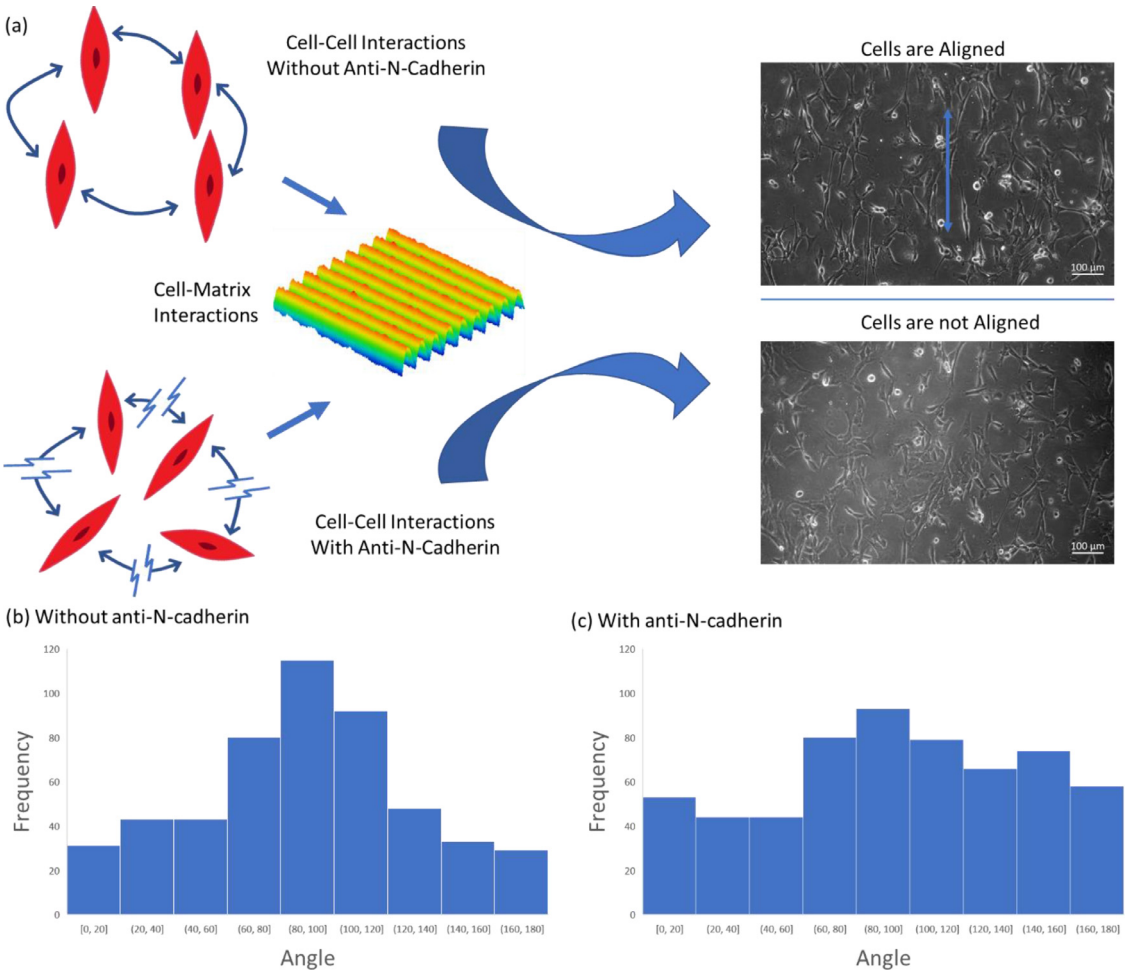

Fig. 1. As cells are cultured onto patterned scaffolds, cell morphology is affected by both cell-matrix and cell-cell interactions. Anti-N-cadherin impacts cell-cell interactions giving rise to differences in cells' sensitivities to wavy surface topographies. (a) Illustration of different cell responses to surface patterns with and without anti-N-cadherin. (b) A histogram of the cell alignment measurements when cultured on a wavy surface without anti-N-cadherin. (c) A histogram of the cell alignment measurements when cultured on a wavy surface with anti-N-cadherin. (For interpretation of the references to colour in this figure legend, the reader is referred to the web version of this article.)

We characterized the alignment of cells during timelapse imaging using custom-written software in python and ImageJ (see Supplementary Information). In each frame or image taken an alignment score was assigned based on cell alignment. The alignment score was derived based on the angle individual cells in an image which were determined ImageJ. The ImageJ plug-in PHANTAST was also used to compare cell confluency of an image to its cell alignment score since confluency impacts cell alignment [28]. Calculating both the confluency of cells and an alignment score for each image or frame from in a timelapse video, allowed us to directly compare the correlation between the two. All experiments of cells with or without the antibody on samples with either the wavelengths 0.56 μm, 0.83 μm, 1 μm and 2 μm were replicated at least 3 times.

2.3. Immunostaining

C2C12 mouse myoblast cells were cultured at 37 °C with 5% CO2 in DMEM (Gibco 11,995,065) supplemented with 10% FBS (GE HyClone SV30160.03HI). Cells were trypsinized, counted with a hemocytometer, then seeded onto substrates in complete growth media at densities of 4000 cells/cm^2 and 32,000 cells/cm^2 for low- and high-density conditions, respectively. Cells were allowed to attach and grow on the substrates for 18–20 h and were subsequently fixed in warm 4% formaldehyde for 15 min, permeabilized in 0.2% Triton X-100 for 10 min, blocked in 1% bovine serum albumin (BSA) for 1 hour, incubated with primary antibodies diluted in 1% BSA for 1 hour (anti-vinculin, clone hVIN-1, Sigma-Aldrich V9131, 1:200), incubated with secondary antibodies diluted in 1% BSA (Thermo Fisher A11031, 1:400) and phalloidin (abcam ab176753, 1:400) for 1 hour, stained with 1 μM DAPI (abcam ab228549) for 5 min, and mounted for microscopy (ProLong Gold Antifade mountant, Thermo Fisher P10144, or 90% glycerol). Between each treatment in staining, cells were washed thrice with PBS with 5 min between each wash.

2.4. Immunostaining imaging and data analysis

Fluorescence microscopy was performed with either Nikon Ti-U (Nikon Plan Fluor 40x/0.75 objective, Nikon Intensilight C–HGFI light source, pco.panda 4.2 sCMOS camera, NIS-Elements D software, 162.5 nm/pixel, 2044 × 2048 pixels, and 0.11 mm^2 image size, for large-scale cell alignment imaging, Fig. 3) or a Zeiss Axio Observer Z1 (EC Plan-Neofluar 100x/1.3 oil objective, HXP 120C light source, AxioCam MRm CCD camera, Zen 2 software, 64.5 nm/pixel and 1388 × 1040 pixel image size, for high-resolution focal adhesion imaging, Fig. 4) inverted epifluorescence microscope setups. Fields of view were randomly chosen throughout the samples.

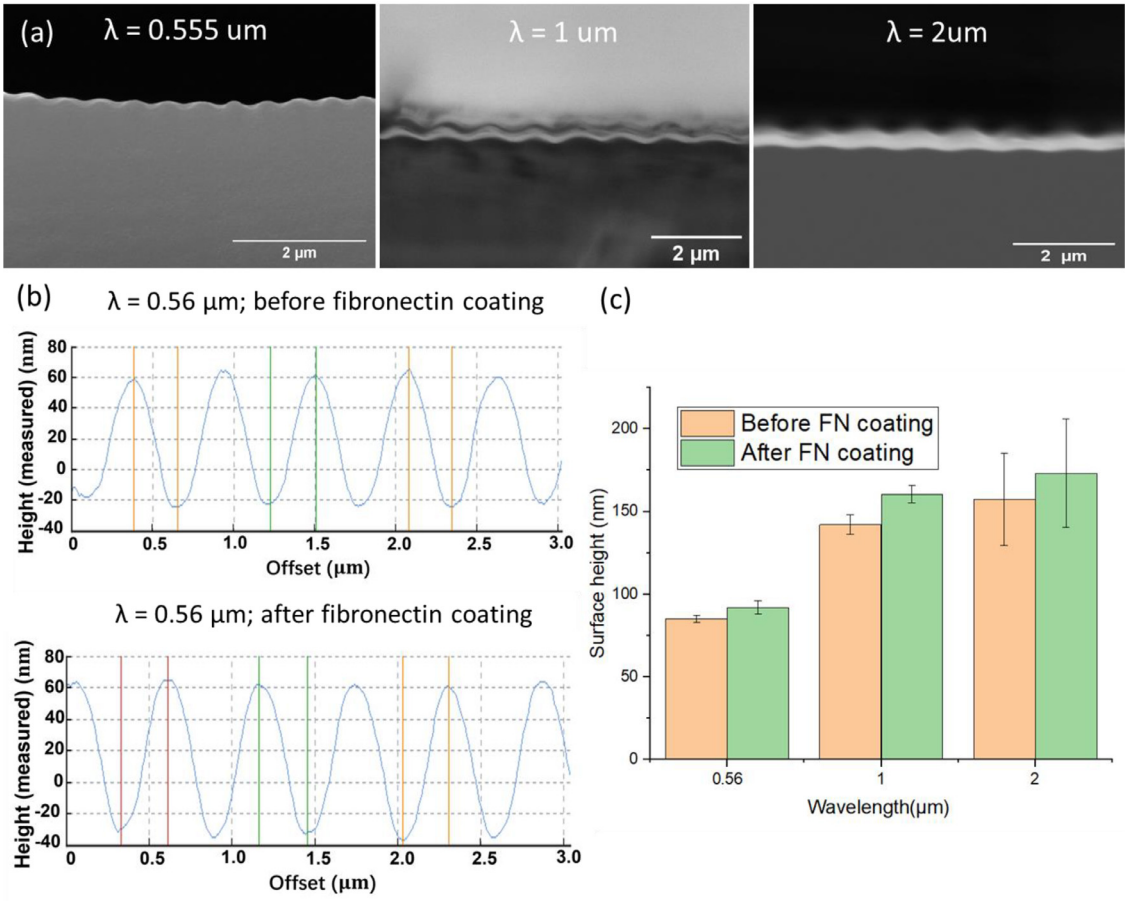

Fig. 2. SEM images (a) of the cross section of each surface pattern on PDMS before fibronectin coating. The surface is facing upward in each SEM image. AFM images of surface profile (b) and bar chart (c) of patterned side of PDMS scaffolds. The surface profile and bar chart compares AFM data before and after fibronectin coating. The sinusoidal periodic patterns can be described by their wavelength λ, and surface height d. Error bars represent standard deviations of measured surface height of $n = 18$ for each profile. (For interpretation of the references to colour in this figure legend, the reader is referred to the web version of this article.)

Immunostaining data was analyzed using custom-written Python programs. Briefly, the local orientation of actin at each pixel was determined from phalloidin images using the gradient structure tensor weighted by a Gaussian with 5 pixel (813 nm) standard deviation; pixels with coherence (difference of eigenvalues divided by the sum of eigenvalues) less than 0.4 were discarded. Nuclei in each field of view were counted from DAPI images by binarizing the image, taking a distance transform on the binarized image, and employing a watershed algorithm on the distance transform. The nematic order parameter for a field of view was calculated similar to Gupta et al. as $S=<\cos[2(\theta-\pi/2)]>$, where θ is the local angle of actin at each pixel from groove direction and the average was weighted by the fluorescence intensity at each pixel [30].

2.5. Atomic force microscopy (AFM) and scanning electron microscope (SEM)

Before cell culture, the topography of bare cell scaffolds was characterized by AFM using an Asylum Research MFP-3D Infinity system under both dry and aqueous conditions. Characterization of topography of surfaces used in timelapse imaging were in dry environment using an Asylum Research MFP-3D Infinity system. Standard Tapping AFM tips used for surface characterization had a full cone angle of 40° and tip radius of < 8 nm. The AFM cantilever had a force constant of 40 N/m and resonance frequency of 325 kHz (NanoAndMore USA HQ:NSC15/Al BS). The scan area was 100 μm^2 with 256 × 256 points. To ensure the quality of surface patterns upon coating ECM, surfaces are characterized by AFM both before and after coating of fibronectin in buffer solution (Fig. 2b, c). The probe used had a force constant of 0.350 N/m and a resonance frequency of 65 kHz (Bruker DNP-S10). Measurements of the surface height of wavy topographies with wavelength 0.56 μm, 1 μm, 2 μm was repeated for 3 regions for 6 different samples. Detailed images and data of the characterization of the wavy surface topography are given in the Supplementary Materials (Fig. S3, S4, S5). The AFM and SEM images of wavy surface with wavelengths 0.56 μm, 1 μm, and 2 μm are shown in Fig. 2. SEM images were acquired using a Quanta 600 Environmental Scanning Electron Microscope with energy-dispersive X-ray and Orientation Imaging Microscopy.

2.6. Alignment sensitivity parameter of scaffolds

A non-dimensional parameter Φ, referred to as the alignment sensitivity parameter by Grigola et al. [17], was used to characterize the geometric features of the wavy patterns:

$$\Phi = \sqrt{\frac{\lambda d}{L^2}} \Big/ \left(1 + \frac{k^{-1}}{L}\right)$$

where λ is the wavelength, d is the amplitude, and κ is the effective curvature of the sinusoidal surface, and L is the size of typical cells when as they spread [17]. The alignment sensitivity parameter correlates with the likelihood of cell alignment on a given smooth, curved sinusoidal topography. The effective curvature, κ, is proportional to the curvature for sinusoidal patterns, which is d/λ^2. For

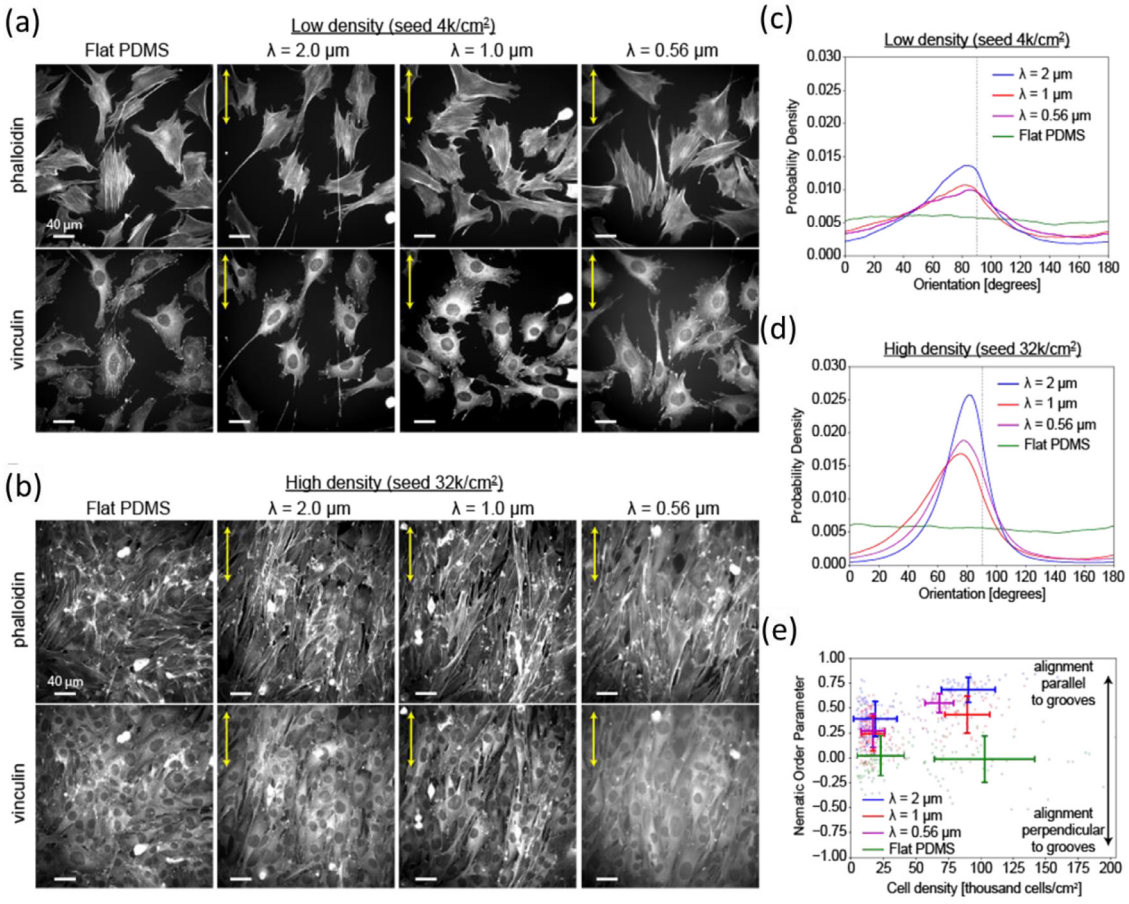

Fig. 3. Cells exhibit large-scale alignment along the direction of the sinusoidal topography. (a) Cells seeded at low density on flat PDMS and sinusoidal topographies of 2 μm, 1 μm, and 0.56 μm (left to right), stained for actin (top) and vinculin (bottom). Groove direction is vertical and indicated by the yellow arrows. (b) Similar as (a) except for cells seeded at high density. (c) Probability density of actin orientation for flat PDMS (green) and sinusoidal topographies with wavelength 2 μm (blue), 1 μm (red), and 0.56 μm (magenta) for cells seeded at low density. Black dashed line indicates vertical direction. Data is merged from 2 independent experiments and 94 fields of view per condition. (d) Same as panel (C) except for cells seeded at high density. Data is from one experiment and 50 fields of view per condition. (e) Scatterplot showing the nematic order parameter versus the cell density for each field of view. Solid lines indicate the mean and standard deviation for each condition. Scale bars: 40 μm. (For interpretation of the references to colour in this figure legend, the reader is referred to the web version of this article.)

a fixed d, as the λ becomes larger, the effective curvature term in the denominator begins to dominate. This captures the fact that the surface appears effectively flat to an individual cell as the effective curvature value approaches 0 either by decreasing d or increasing λ. A cell length dimension for C2C12 cells of $L = 60$ μm was chosen to nondimensionalize the data related to the alignment sensitivity parameter. Grigola et al. showed that the cell alignment behavior is relatively insensitive to the selection of L [17].

2.7. Statistical analysis

The data in this study are expressed as mean and error bars that represent ± standard deviation. In order to evaluate statistically significant differences in cell alignment with or without anti-N-cadherin, an F-test was used to determine significant variance between groups and defined as P values less than 0.05.

3. Results

3.1. Cell alignment and cell density

Cells were seeded at low and high densities, allowed to grow for 18–20 hour, then immunostaining was performed to visualize vinculin, a cell-substrate and cell-cell adhesion protein, and actin (Fig. 3a, b). We quantified the local orientation of actin at each pixel in an image as a proxy for the global cell alignment and correlated this with the observed cell density by counting the number of cell nuclei. On flat PDMS substrates, no preferential alignment was observed. On sinusoidal topographies, at low densities we observed slight bias in alignment along the direction of the grooves in all the wavelengths tested, with 2 μm wavelength providing the strongest bias (Fig. 3a, c). At high densities, the alignment along the groove direction was significantly enhanced in all wavelengths (Fig. 3b, d, e). This result was consistent with previous work [17], both in that cell alignment was enhanced on the longest wavelength substrate and at higher cell densities.

On sinusoidal topographies and at low cell densities, we observed two distinct types of cell-substrate adhesions (Fig. 4a). The first type was aligned along the direction of the grooves, which had a lateral spacing consistent with the wavelength of the grooves and were larger for 2 μm wavelength grooves and correspondingly smaller for 1 μm and 0.56 μm wavelengths grooves. These adhesions were prevalent on lamellipodia-like protrusions. The second type was angled with respect to the groove direction, either diagonally or orthogonally, and for 2 μm wavelength grooves were often discontinuous while cells on 1 μm and 0.56 μm wavelength grooves were able to form large, continuous focal adhesions. These larger, thicker focal adhesions were usually associated with actin stress fibers. As the cell density increased and cells aligned along the direction of grooves, these large, angled focal adhesion complexes were no longer visible on any sinusoidal substrate. The only

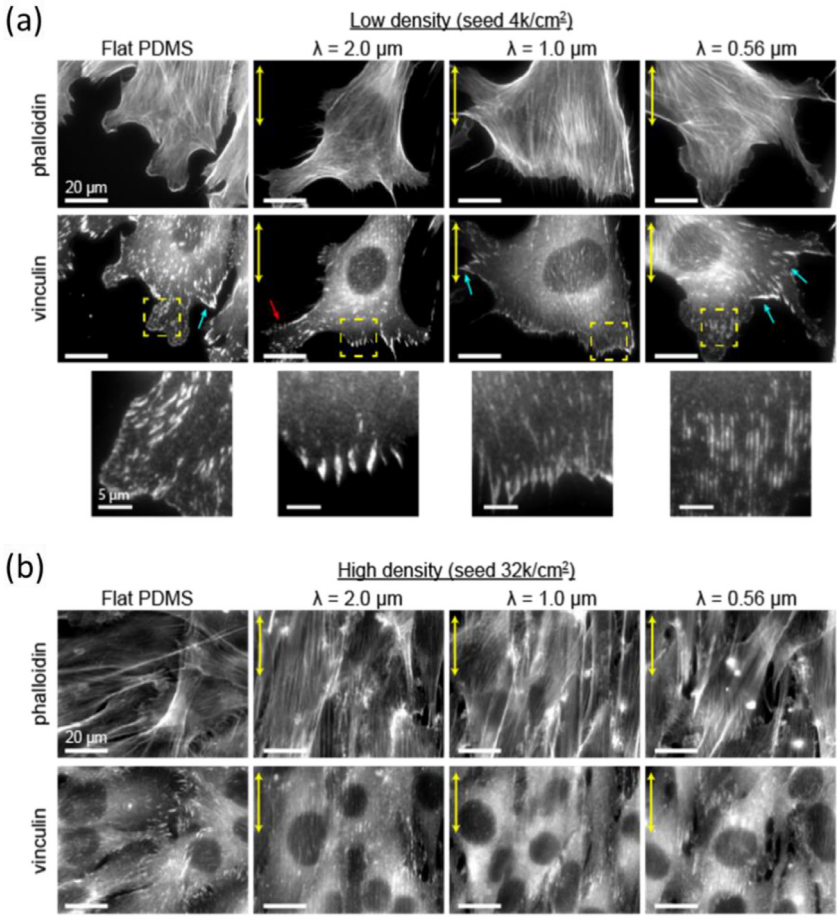

Fig. 4. Focal adhesion morphology on sinusoidal topographies. (a) Cells seeded at low density on flat PDMS and sinusoidal wavelengths of 2 μm, 1 μm, and 0.56 μm (left to right), stained for actin (top) and vinculin (middle). The groove direction is vertical and indicated by the yellow arrows. Zoomed inset areas are shown in yellow boxes. Cyan arrows indicate focal adhesions which form at an angle to the grooves, while red arrow indicates adhesion which is oriented at an angle relative to the groove but is discontinuous. (b) Similar as (a) except for cells seeded at high density. Scale bars: 20 μm, or 5 μm (insets). (For interpretation of the references to colour in this figure legend, the reader is referred to the web version of this article.)

cell-substrate adhesions that remained were largely oriented parallel to the grooves (Fig. 4b). Cells seeded onto flat PDMS substrates could form large focal adhesion complexes in any direction, even at higher cell densities.

3.2. Quantifying cell alignment

Cells were cultured on sinusoidal patterned surfaces. The alignment sensitivity parameter, Φ, was used to characterize the likelihood of cell alignment on a smooth sinusoidal topography for a given wavelength and amplitude. Grigola et al. found that when $0.01 < \Phi < 0.1$, cells exhibited greater alignment on sinusoidal surfaces as confluency increased and when $\Phi > 0.1$, cells exhibited strong polarization regardless of cell confluency. We utilized anti-N-cadherin to perturbed cell-cell interactions on topographies where confluency promotes alignment. At the same confluency, cells cultured in the presence of anti-N-cadherin exhibited lower alignment on surfaces with where $0.01 < \Phi < 0.1$ (Fig. 5a). On surfaces where $\Phi > 0.1$, there was little difference in cell alignment between cells in the presence of anti-N-cadherin verses without (Fig. 5b).

3.3. Quantifying cell motility

Time lapse imaging of cells on scaffolds has been used in fields varying from gene expression analysis to 3D tissue formation [29]. For our work, time lapse videos were captured of cells cultured on various surface topographies for tracking motility and overall culture organization. In Fig. 6, C2C12 cells were cultured on flat (Fig. 6a, c, e) and patterned (Fig. 6b, d, f) surfaces for characterization. In each time lapse video 10 cells were tracked to measure their position (Fig. 6a, b) and instantaneous angle (Fig. 6c, d). The centroid of each cell was manually tracked to determine the position of cells over 72 h. To better quantify these results, the motility of cells was tracked by N number of points where $pi = (x_i, y_i)$ is the position of a cell. The instantaneous angle is the most recent displacement vector from the previous N point to the current N point of the tracked cell. The instantaneous angle is defined by $\alpha = \arctan [(y_{i+1} - y_i)/(x_{i+1} - x_i)]$.

To compare models of high verses low cell alignment, cell responses on flat (Fig. 6a, c, e) or patterned surface with $\Phi > 0.01$ (Fig. 6b, d, f) were compared. Tracking motility of cells cultured on a flat surface exhibited no preferential orientation for movement, and the instantaneous angle measured as the cells migrate is nearly random, giving rise to a broad scattering of migration direction (Fig. 6a, c, e). On the other hand, on the patterned surface with $\Phi > 0.01$, cells migrate along the direction of the microgroove channels, leading to a strongly preferred direction of migration, as demonstrated in Fig. 6b, d, f.

To investigate the role of cell-cell interactions in cell responses to patterned surfaces, cells were cultured on the same surface in the presence (Fig. 7a; mmc2) or absence (Fig. 7b; mmc3) of anti-

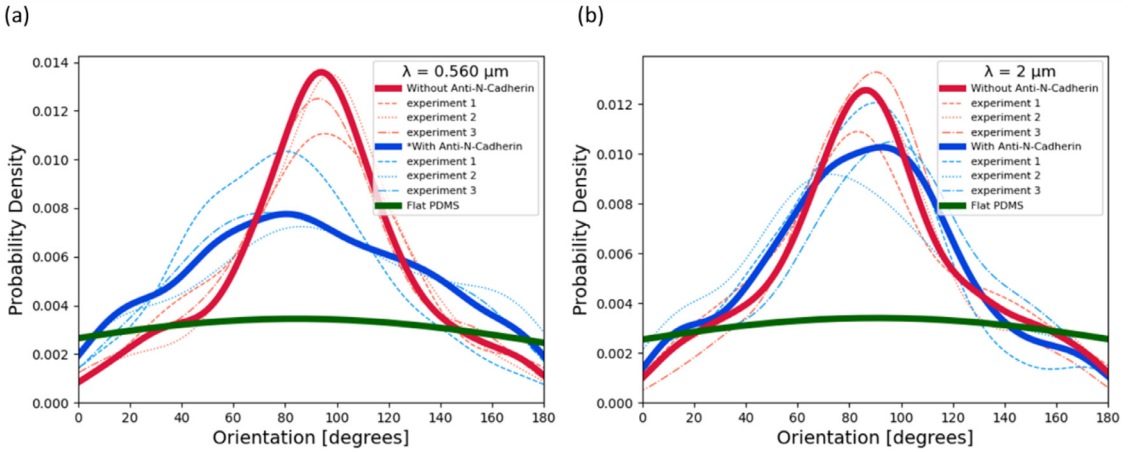

Fig. 5. Probability density function of cell orientation when cultured on micro patterned PDMS with $\lambda = 0.56$ µm (a) and $\lambda = 2$ µm (b). At each wavelength cells orientation was compared when cell culture was with (blue) or without anti-N-cadherin (red). Solid lines are combined probability density functions of dashed lines from individual experiments. Cell orientation was compared when confluency reached 41±6% ($n = 3$). Green line is probability density function of flat PDMS. Flat PDMS data was used for both $\lambda = 0.56$ µm and $\lambda = 2$ µm. When $\lambda = 2$ µm, $\Phi > 0.01$. When $\lambda = 0.56$ µm, $0.001 < \Phi < 0.01$. $^*P < 0.05$ versus normal C2C12 cell culture on the same wavelength. (For interpretation of the references to colour in this figure legend, the reader is referred to the web version of this article.)

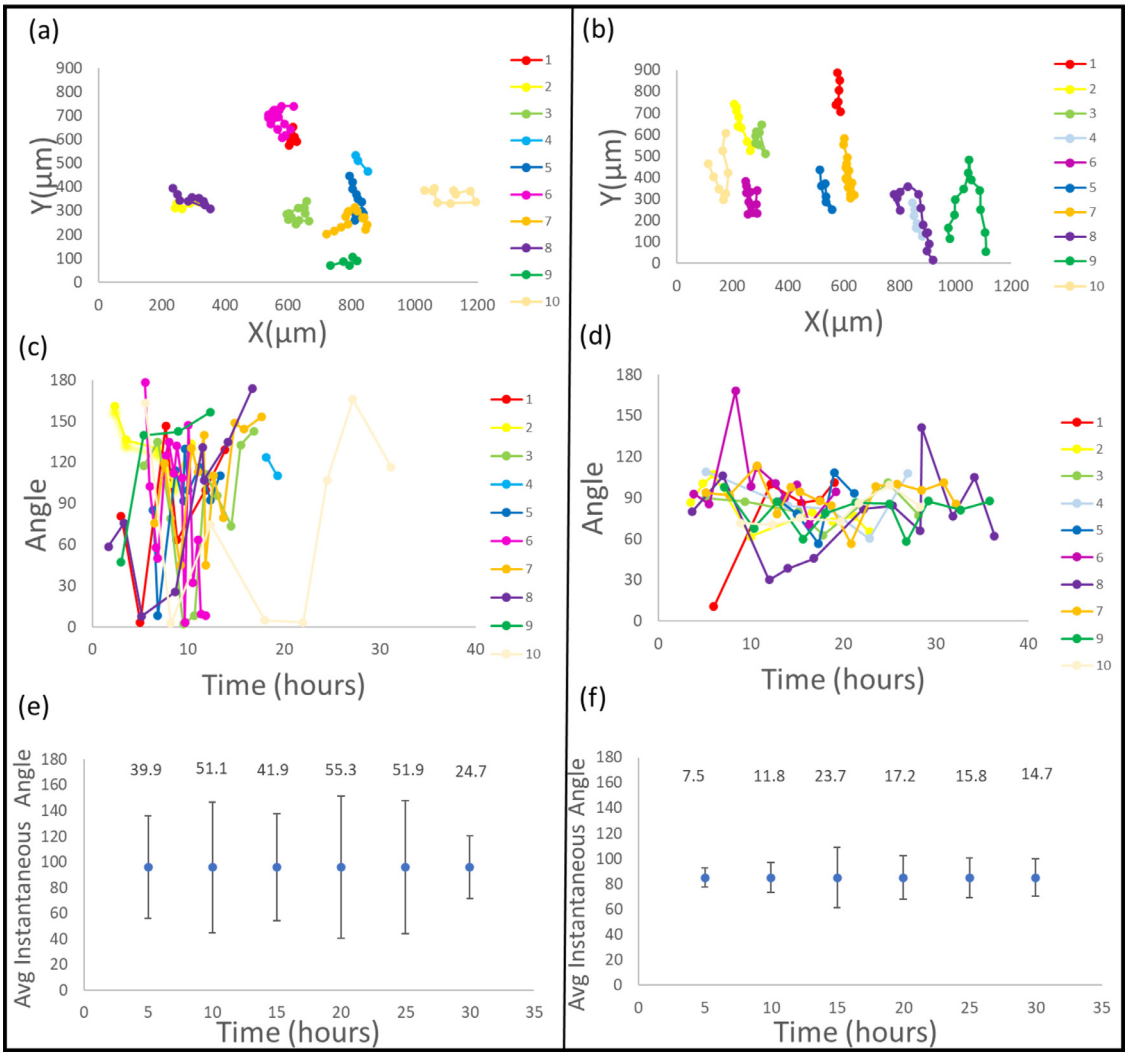

Fig. 6. The position (a, b), angle (c, d), and instantaneous angle change (e, f) were tracked for ten randomly selected cells cultured on a flat (a, c, e) vs patterned surface ($\lambda = 2$ µm, $d = 450$ nm, $\varphi = 0.0138$) (b, d, f). Cell motility was tracked from the beginning to end of their cell cycle. The displacement vector is the instantaneous angle of cells between cell positions in each frame. Cell movements to the right is 0° and to the left is 180° Movement up or down is 90° The error bars (e, f) represent the standard deviation of the instantaneous angle. (For interpretation of the references to colour in this figure legend, the reader is referred to the web version of this article.)

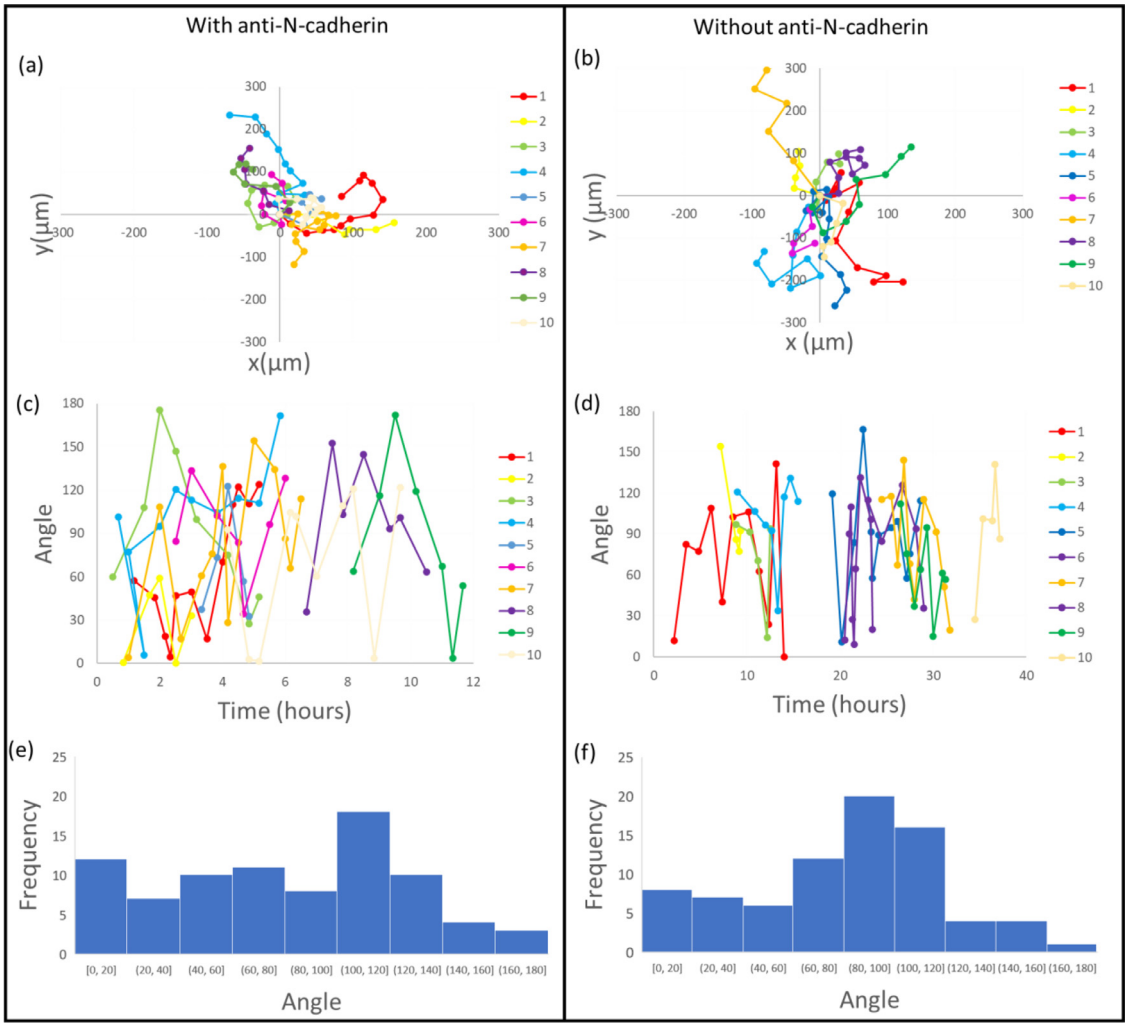

Fig. 7. Cells were cultured on the same surface in the presence (a, c, e) and absence (b, d, f) of anti-N-cadherin on a scaffold with a sinusoidal wavy topography (λ=0.83 μm, d = 77 nm, and Φ=0.004). The cell position (a, b), instantaneous angle (c, d), and a histogram of all instantaneous angles (e, f) were compared between cells cultured with and without anti-N-cadherin. Cells in the presence of anti-N-cadherin were less polarized and exhibited a lower degree of alignment than cells cultured without anti-N-cadherin. (For interpretation of the references to colour in this figure legend, the reader is referred to the web version of this article.)

N-cadherin. By tracking the cell positions throughout its cell-cycle, cells cultured without anti-N-cadherin exhibited greater preferential movement along the microgroove channels. A histogram of the instantaneous angle between cell positions was more uniformly distributed for cells cultured with anti-N-cadherin than without the antibody (Fig. 7e, f).

3.4. Role of cell-matrix interaction in cell-alignment

Cell responses to patterned surface features are modulated by cell-matrix interactions and mechanotransduction via scaffold geometries. Mechanical cues from scaffold geometries influence overall cell culture organization via cell-surface receptors which initiate intracellular responses related to cell motility and morphology [30]. Scaffold surface geometries with a Φ greater than 0.01 induce individual cell alignment via cell-surface receptors [8,17]. Cells cultured with or without anti-N-cadherin on surfaces with a Φ greater than 0.01 exhibited no difference in cell alignment behavior throughout cell proliferation (Fig. 8a). On the other hand, cells interfacing with scaffolds with a value of Φ less than 0.001 would not align regardless of cell confluency, similar to cell responses on a flat surface [17]. It is likely that, below the Φ threshold of 0.001, cell-surface receptors would not sense the patterned surface and responded to surface topography because the surface is essentially flat [17].

3.5. Role of cell-cell interaction in cell-alignment

When Φ is between 0.001 and 0.01, the necessity for cell confluency to achieve cell alignment suggests that cell-cell interactions enhance sensitivity of cell-matrix interactions, which could be through a variety of molecular mechanisms [31]. Isolating the role of intracellular and intercellular responses can inform cell alignment's dependence on cell-cell and cell-matrix interactions. To examine phenotypic responses to cell-cell and cell-matrix interactions, anti-N-cadherin was utilized to examine the role of cell-cell interactions in cell culture related to surface topography. The selected anti-body inhibits cell-cell junctions by specifically binding to several locations on the extracellular domain of the protein [31–33]. Inhibiting the adhesion molecule has an important role in the biochemical pathways of intercellular responses by mediating calcium-dependent homophilic cell-cell interactions [31]. When Φ was between 0.001 and 0.01 and cells were in the presence of anti-N-cadherin, cells required a greater percentage of confluency in order to align with the microgroove channels (Fig. 8b).

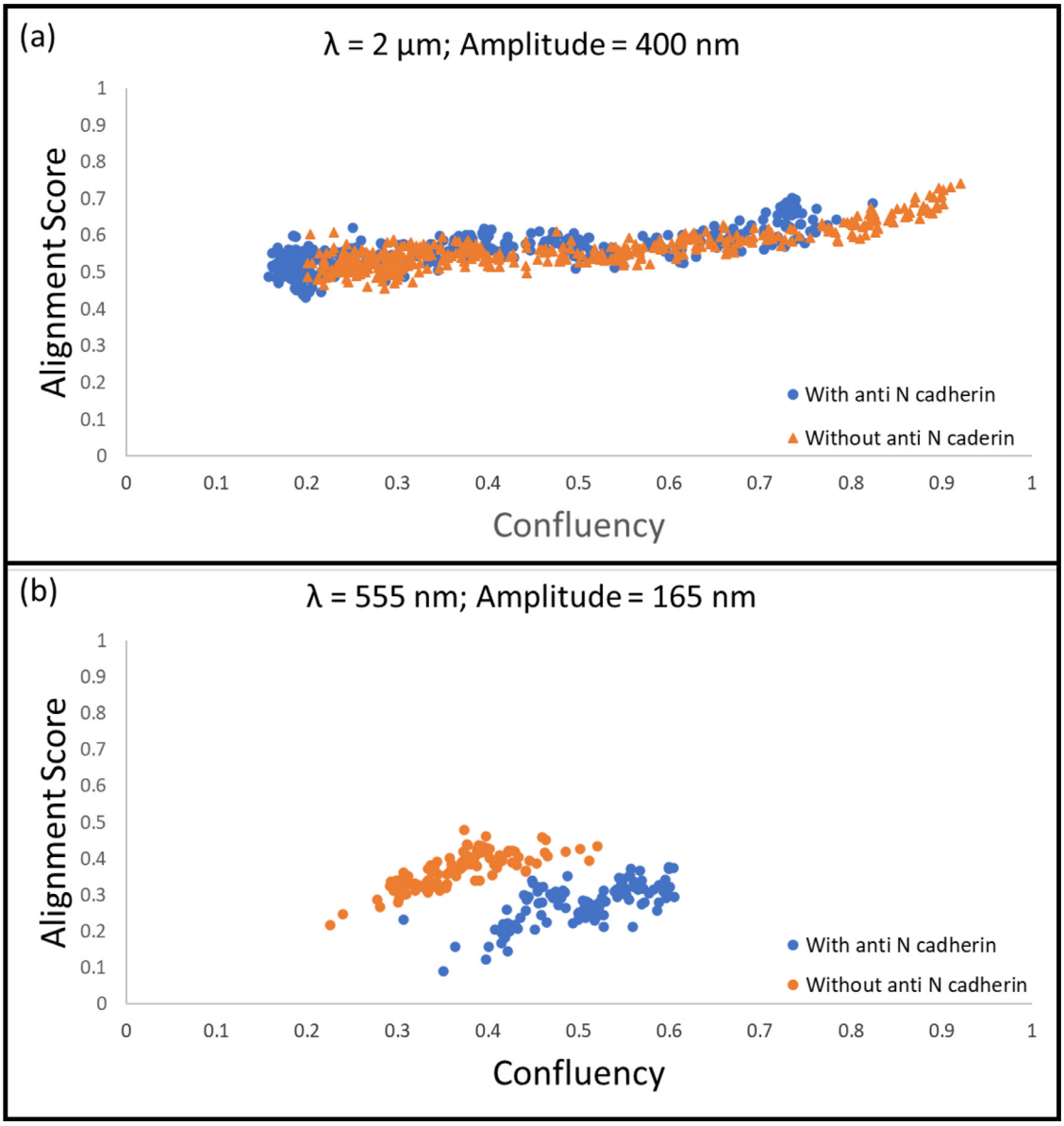

Fig. 8. Time lapse videos that compared cells cultured with or without anti-N-cadherin on the same surface with a Φ greater than 0.01 (a), had a similar trend in net alignment, regardless of confluency. Cells cultured on the same surface when Φ value was between 0.001 and 0.01 (b), showed a direct relationship between cell alignment and cell confluency. Cells cultured in the presence of anti-N-cadherin required greater confluency to have the same alignment score (b). (For interpretation of the references to colour in this figure legend, the reader is referred to the web version of this article.)

4. Discussion

In addition to our focus on surface topography, it is important to note the role of fibronectin as ECM in facilitating mechanotransduction via focal adhesions. C2C12 myoblasts grown on fibronectin show greater cell alignment than on laminin or gelatin and greater collective directional migratory behavior than gelatin in vitro [34]. This is likely because fibronectin is recognized by many different cell-surface receptors of the transmembrane integrin family [35,36]. Many of these focal adhesion binding sites in fibronectin are RGD peptide specific [37]. One study by Vaz et al. found that inhibiting RGD-binding integrins with GRGDS peptide resulted in complete detachment of C2C12 cells from fibronectin-coated glass coverslips [34]. Fibronectin and RGD-binding integrins in C2C12 cells, such as $\alpha 5\beta 1$, $\alpha v\beta 1$, and $\alpha v\beta 3$, constitute a primary pathway for intracellular force transmission [34,36,37].

The mechanisms suggest that the observed anisotropy in cell morphology and collective migratory behavior may originate from the prestress residing in intracellular stress fibers orientated preferienitally along the long axis of the cells [38]. Observed differences in actin fiber and focal adhesion alignment between cells cultured on patterned verse flat PDMS helped illuminate the role of cell-matrix adhesion and cell alignment (Figs. 3 and 4). Actin fiber alignment is relevant because cell moltility is initiated by actin-dependant lamellipodia along the cells leading edge, followed by the cell body being pushed forward through intracellular contraction forces [39,40]. The dependence of cell alignment to matrix topography suggests cell sensitivity to cell alignment is, in part, dependant on physical phenomena. While cell-matrix adhesions helps elucidates the role of mechanotransduction and cell alignment in 2D, studies have shown that cells in a 3D matrix interact with distinct behaviors to that of adhesions formed in a 2D matrix [41].

There are many pathways of cell signaling that are activated by various cadherin-mediated cell-cell contacts. These cadherins are crucial in mediating homophilic cell-cell adhesions and facilitating cell proliferation, fusion, and maturation. While much about cell signaling is unknown, recent studies suggest downstream signals from cadherin-mediated contacts are both cadherin-specific and cell-context-specific [42]. Well studied cadherins of C2C12 cells such as M-cadherin, R-cadherin, E-cadherin, and N-cadherin have cell-context-specific roles during proliferation and differentiation in vitro. Increased expression of R-cadherin results in myogenesis inhibition and myoblast transformation [43]. In addition, the expression of R-cadherin is accompanied by a delocalization at the membrane junction of the endogenous expression of N-cadherin and M-cadherin [43]. A study by Ozawa, found expressing E-cadherin cytoplasmic domain ectopically in C2C12 myoblasts inhibits cell-cell fusion and elicits delocalization of M-cadherin and N-cadherin [44]. All these cadherin-mediated contacts activate the Rho family of GTPases, which play a critical role in cytoskeleton-dependent cell functions, such as cell morphology [45]. Although knocking out or inhibiting a specific cadherin cell-cell contacts is not sufficient to abrogate its specific function, several downstream signals mediating by cell morphology and proliferation are still perturbed. This study focused on the inhibition of N-cadherin since it affects RhoA activation, which is believed to regulate cytoskeleton morphology and cell motility distally from the cell surface [46,47].

In addition to our study that suggests cell-cell communication promotes cell alignment, other studies have shown cell-cell communication regulates myogenesis in C2C12 cells [48]. While the focus of this study is of cell alignment in 2D, the transition from 2D to 3D cell alignment offers another dimension of complexity more comparable to in vivo conditions. Isolating the role of cell-cell verses cell-matrix interactions is more complex as there are differences in adhesion protein expression of two- versus three-dimensional cultures in vitro [49].

Insights of cell-cell interactions in this study are particularly relevant in informing future scaffold designs in the fields of tissue engineering, regenerative medicine, and cell-based soft robotics. We found that cell-cell interactions promote alignment on smaller wavy patterns, that individual cells do not align on. Perturbing cell-cell attachment of confluent cultures on smaller wavy patterns inhibits cell alignment, meaning that smaller patterns on scaffolds can achieve cell alignment at the right confluency. This can be useful in fields such as biohybrid robotics, where micro-scale mechanics are important considerations in promoting actuation via aligned muscle cells [3,50].

5. Conclusion

Cell-cell interactions play an important role in cell alignment in 2D culture especially when examining surface topography. We probed how cell confluency and cell-cell interactions impact cell alignment on different surface topographies. We first developed an approach to fabricate wavy topographies for cell culture. Then we captured time lapse videos of cells cultured on wavy topographies to investigate the role of cell-cell interactions and cell alignment. We found that cell-cell interactions can be altered through anti-N-cadherin. On surfaces with sensitivity parameter, Φ, ranging between 0.001 and 0.01, when cells were more confluent, they were better aligned along the channels of the anisotropic sinusoidal wavy patterns. However, cells in the presence of anti-N-cadherin required higher confluency than cells without anti-N-cadherin to be aligned (Fig. 8b). On surfaces with Φ greater than 0.01, cell alignment was not dependent on confluency and the cells were aligned even at low percentages of confluency. We observed no difference between cell cultures with and without anti-N-cadherin when the value of Φ was greater than 0.01. To our knowledge, our study is the first to show the difference that cell-cell interactions make in promoting cell alignment on wavy topographies to which cells are otherwise not responsive. Further studies that isolate the role of cell-cell and cell-matrix interactions in cellular organization will inform the role of mechanotransduction in developmental biology, especially in 3D culture.

Declaration of Competing Interest

The authors declare that they have no financial interests or personal relationships that could influence the work reported in this paper.

Acknowledgements

The authors would like to acknowledge use of the Materials Characterization Facility at Carnegie Mellon University (MCF-677785). This work was supported in part by the National Institute of Health (R01AG06100501A1), Air Force Office of Scientific Research (FA9550–18–1-0262), National Science Foundation (CMMI-1946456), Office of Naval Research (N00014-17–1–2566), and the Pennsylvania Department of Health (SAP4100077084). BD and KJH acknowledge partial financial support by the NIH Eunice Kennedy Shriver National Institute of Child Health and Human Development (grant R01HD086325). KJH, YH and HRS would like to acknowledge the financial support from Nanyang Technological University (grant M4082428.050). HRS would like to thank the URECA Program at Nanyang Technological University. We thank the Advanced Biofilm Imaging Facility at the (SCELSE) for providing the Zeiss Axio Observer Z1 microscope setup.

Supplementary materials

Supplementary material associated with this article can be found, in the online version, at doi:10.1016/j.actbio.2022.01.057.

References

[1] K. Matsuura, R. Utoh, K. Nagase, T. Okano, Cell sheet approach for tissue engineering and regenerative medicine, J. Controlled Release (2014) 228–236.
[2] X. Liu, P.X. Ma, Polymeric Scaffolds for Bone Tissue Engineering, Biomed. Eng. Soc. (2004) 477–486.
[3] S. Coyle, C. Majidi, P.R. LeDuc, K.J. Hsia, Bio-inspired soft robotics: material selection, actuation, and design, Extreme Mech. Lett. 22 (2018) 51–59.
[4] Y. Sawa, S. Miyagawa, T. Sakaguchi, T. Fuhita, A. Matsuyama, A. Saito, T. Shimizu, T. Okano, Tissue engineered myoblast sheets improved cardiac function sufficiently to discontinue LVAS in a patient with DCM: report of a case, Surg. Today 42 (2) (2012) 181–184.
[5] N.G. Rim, A. Yih, P. Hsi, Y. Wang, Y. Zhang, J.Y. Wong, Micropatterned cell sheets as structural building blocks for biomimetic vascular patches, Biomaterials 181 (2018) 126–139.
[6] S. Chien, Mechanotransduction and endothelial cell homeostasis: the wisdom of the cell, Heart Circulaotry Physiol. 292 (3) (2007).
[7] M.N. Andalib, Y. Dzenis, H.J. Donahue, J.Y. Lim, Biomimetic substrate control of cellular mechanotransduction, Biomater. Res. 20 (11) (2016).
[8] C.-.M. Cheng, R.L. Steward Jr., P.R. LeDuc, Probing cell structure by controlling the mechanical environment with cell–substrate interactions, J. Biomech. (2009) 187–192.
[9] R.L. Steward, C.-.M. Cheng, D.L. Wang, P.R. LeDuc, Probing Cell Structure Responses Through a Shear and Stretching Mechanical Stimulation Technique, Cell Biochem. Biophys. 56 (2010) 115–124.
[10] C. He, M. Liu, D. Jiang, C. Qin, T. Liang, P. Wu, C. Han, L. Huang, K.J. Hsia, P. Wang, Controlling cellular arrangements via stretched bioprinting, bioRxiv (2020).
[11] A.L. Berrier, K.M. Yamada, Cell–Matrix Adhesion, J. Cell. Physiol. 213 (2007) 565–573.
[12] J. Hu, C. Hardy, C.-.M. Chen, S. Yang, A.S. Voloshin, Y. Liu, Enhanced Cell Adhesion and Alignment on Micro-Wavy Patterned Surfaces Jia, PLoS One (2014).
[13] W.-J. Li, R.L. Mauck, J.A. Cooper, X. Yuan, R.S. Tuan, Engineering controllable anisotropy in electrospun biodegradable nanofibrous scaffolds for musculoskeletal tissue engineering, J. Biomech. 40 (8) (2007) 1686–1693.
[14] D. Joaquin, M. Grigola, G. Kwon, C. Blasius, Y. Han, D. Perlitz, J. Jiang, Y. Ziegler, A. Nardulli, K.J. Hsia, Cell migration and organization in three-dimensional in vitro culture driven by stiffness gradient, Biotechnol. Bioeng. 113 (11) (2016) 2496–2506.

[15] M. Gupta, B.L. Doss, L. Kocgozlu, M. Pan, R.-.M. Mège, A. Callan-Jones, R. Voituriez, B. Ladoux, Cell shape and substrate stiffness drive actin-based cell polarity, Phys. Rev. 99 (1) (2019) 012412.
[16] X. Jiang, S. Takayama, X. Qian, E. Ostuni, H. Wu, N. Bowden, P. LeDuc, D.E. Ingber, G.M. Whitesides, "Controlling Mammalian Cell Spreading and Cytoskeletal Arrangement with Conveniently Fabricated Continusous Wavy Features on Poly(dimethylsiloxane)," American Chemical Society (2002), pp. 3273–3280.
[17] M.S. Grigola, C.L. Dyck, D.S. Babacan, D.N. Joaquin, K.J. Hsia, Myoblast Alignment on 2D Wavy Patterns: dependence on Feature Characteristics and Cell–Cell Interaction, Biotechnol. Bioeng. (2014) 1617–1626.
[18] M.A. Hill, G.A. Meininger, Myogenic Tone and Mechanotransduction, Muscle 2 (2012) 1243–1257.
[19] R. Janostiak, A.C. Paraki, J. Brabek, D. Rosel, Mechanosensors in integrin signaling: the emerging role of p130Cas, Eur. J. Cell Biol. 93 (10–12) (2014) 445–454.
[20] A.w. Orr, B.P. Helmke, B.R. Blackman, M.A. Schwartz, Mechanisms of Mechanotransduction, Dev. Cell 10 (1) (2006) 11–20.
[21] Y. Chen, L. Ju, M. Rushdi, C. Ge, C. Zhu, Receptor-mediated cell mechanosensing, Mol. Biol. Cell 28 (23) (2017) 3134–3155.
[22] D. Mohammed, M. Versaevel, C. Bruyere, L. Alaimo, M. Luciano, E. Vercruysse, A. Proces, S. Gabriele, "Innovative Tools for Mechanobiology: unraveling Outside-In and Inside-Out Mechanotransduction," frontiers in Bioengineering and Biotechnology, 7 (162), 219.
[23] A. Cipitria, M. Salmeron-Sanchez, Mechanotransduction and Growth Factor Signalling to Engineer Cellular Microenvironments, Adv. Healthc. Mater. 6 (15) (2017).
[24] S. Yang, K. Khare, P.C. Lin, Harnessing surface wrinkle patterns in soft matter, Adv. Funct. Mater. 20 (16) (2010) 2550–2564.
[25] F.A. Bayley, J.L. Liao, P.N. Stavrinou, A. Chiche, J.T. Cabral, Wavefront kinetics of plasma oxidation of polydimethylsiloxane: limits for sub-μm wrinkling, Soft Matter 10 (8) (2014) 1155.
[26] H. Hu, C. Huang, Xiao Hu Liu, K.J. Hsia, Thin film wrinkling by strain mismatch on 3D surfaces, Extreme Mech. Lett. (2016) 107–113.
[27] E. Meijering, O. Dzyubachyk, I. Small, Methods for Cell and Particle Tracking, Meth. Enzymol. (2012) 183–200.
[28] N. Jaccard, L.D. Griffin, A. Kesar, R.J. Macown, A. Super, F.S. Versaitech, N. Szita, Automated method for the rapid and precise estimation of adherent cell culture characteristics from phase contrast microscopy images, Biotechnol. Bioeng. 111 (3) (2014) 504–517.
[29] P.A. Agudelo-Garcia, J.K.D. Jesus, S.P. Williams, M.O. Nowicki, E.A. Chiocca, S. Liyanarachchi, P.-.K. Li, J.J. Lannutti, J.K. Johnson, S.E. Lawler, M.S. Viapiano, Glioma Cell Migration on Three-dimensional Nanofiber Scaffolds Is Regulated by Substrate Topography and Abolished by Inhibition of STAT3 Signaling, Neoplasia (2011) 831–840.
[30] H. Wolfenson, B. Yang, M.P. Sheetz, Steps in Mechanotransduction, Annu. Rev. Physiol. 81 (2019) 585–605.
[31] S. Charrasse, M. Meriane, F. Comunale, A. Blangy, C. Gauthier-Rouvière, N-cadherin-dependent cell-cell contact regulates Rho GTPases and β-catenin localization in mouse C2C12 myoblasts, J. Cell Biol. 158 (5) (2002) 953–965.
[32] L.D. Derycke, M.E. Bracke, N-cadherin in the spotlight of cell-cell adhesion, differentiation, embryogenesis, invasion and signalling, Int. J. Dev. Biol. 48 (2004) 463–476.
[33] K. Tamura, W.-.S. Shan, W.A. Hendrickson, D.R. Colman, L. Shapiro, Structure–Function Analysis of Cell Adhesionby Neural (N-) Cadherin, Neuron 20 (1998) 1153–1163.
[34] R. Vaz, G.G. Martins, S. Thorsteinsdottir, G. Rodrigues, Fibronectin promotes migration, alignment and fusion in an in vitro myoblast cell model, Cell Tissue Res. 358 (2012) 569–578.
[35] E. Clark, J. Brugge, Integrins and signal transduction pathways: the road taken, Science 268 (5208) (1995) 233–239.
[36] K. Huang, R.D. Kamm, R.T. Lee, "Cell mechanics and mechanotransduction: pathways, probes, and physiology," American Physiological Society, 287 (1) (2004) pp. C1–C11.
[37] S. Johansson, G. Svineng, K. Wennerberg, A. Armulik, L. Lokikangas, Fibronectin-Integrin Interactions, Front. Biosci. 2 (1997) 126–146.
[38] S. Lumetti, S. Mazzotta, S. Ferrillo, M. Piergianni, M. Piemontese, G. Passeri, G.M. Macaluso, C. Galli, RhoA Controls Wnt Upregulation on Microstructured Titanium Surfaces, Biomed. Res. Int. (2014) 9.
[39] K.J. Hsia, in: Role of Mechanics in Biological Materials Research, McGraw-Hill Education, 2009, pp. 319–326.
[40] G. Giannone, B.J. Dublin-Thaler, O. Rossier, Y. Freund, G. Borisy, M.P. Sheetz, Lamellipodial Actin Mechanically Links Myosin Activity with Adhesion-Site Formation, Cell 128 (3) (2007) 561–575.
[41] A.D. Doyle, K.M. Yamada, Mechanosensing via cell-matrix adhesions in 3D microenvironments, Exp. Cell Res. 343 (1) (2016) 60–66.
[42] M.J. Wheelock, K.R. Johnson, Cadherin-mediated cellular signaling, Curr. Opin. Cell Biol. 15 (2003) 509–514.
[43] J. Kucharczak, S. Charrasse, F. Comunale, J. Zappulla, B. Robert, I. Teulon–Navarro, A. Pelegrin, C. Gauthier-Rouviere, R-Cadherin Expression Inhibits Myogenesis and Induces Myoblast Transformation via Rac1 GTPase, Cancer Res. 68 (16) (2008) 6559–6568.
[44] M. Ozawa, E-cadherin cytoplasmic domain inhibits cell surface localization of endogenous cadherins and fusion of C2C12 myoblasts, Company Biologists 4 (2015) 1427–1435.
[45] H. Takano, I. Komuro, T. Oka, I. Shiojima, Y. Hiroi, T. Mizuno, Y. Yazaki, The Rho Family G Proteins Play a Critical Role in Muscle Differentiation, Mol. Cell. Biol. 18 (3) (1998) 1580–1589.
[46] F. Comunale, M. Causeret, C. Fravard, J. Cau, N. Taulet, S. Charrasse, C. Gauthier-Rouviere, Rac1 and RhoA GTPases have antagonistic functions during N–cadherin-dependent cell–cell contact formation in C2C12 myoblasts, Biol. Cell (2007) 503–517.
[47] L. Becciolini, E. Meacci, C. Donati, F. Cencetti, E. Rapizzi, P. Bruni, Sphingosine 1-phosphate inhibits cell migration in C2C12 myoblasts, Biochim. Biophys. Acta 1761 (2006) 43–51.
[48] K. Tanaka, K. Sato, T. Yoshida, T. Fukuda, K. Hanamura, N. Kojima, T. Shirao, T. Yanagawa, H. Watanabe, Evidence for cell density affecting C2C12 myogenesis: possible regulation of myogenesis by cell-cell communication, Muscle Nerve 44 (6) (2011) 968–977.
[49] I. Grabowska, A. Sxeliga, J. Maraczewski, I. Czaplicka, E. Brzoska, Comparison of satellite cell-derived myoblasts and C2C12 differentiation in two- and three-dimensional cultures: changes in adhesion protein expression, Cell Biol. Int. 35 (2011) 125–133.
[50] L. Sun, Y. Yu, Z. Chen, F. Bian, F. Ye, L. Sun, Z. Yuanjin, Biohybrid robotics with living cell actuation, R. Soc. Chem. 49 (2020) 4043–4069.